

國立交通大學

材料科學與工程學系

碩士論文

具有九十奈米側壁閘極之高射頻特性砷化
鎵變異結構高電子遷移率電晶體

**High RF Performance GaAs Metamorphic
HEMTs with 90-nm Sidewall Gate**



研究生：彭怡瑄

指導教授：張翼 博士

中華民國九十三年七月

具有九十奈米側壁閘極之高射頻特性砷化鎵變 異結構高電子遷移率電晶體

研究生：彭怡瑄

指導教授：張翼 博士

國立交通大學材料科學與工程學系

摘 要

就高頻應用而言，為了增進射頻特性，閘極尺寸有越做越小的趨勢。本論文主要的目的是利用側壁堆積法來縮小線寬，利用氧化矽及氮化矽兩種不同介電材料間的連續堆積及蝕刻，製作出奈米尺寸的線寬。另一方面，由於氮化矽與氧化矽之間的高選擇比，讓製程有較佳的再現性及均勻性。因此，我們可以發展出一個易於控制的小線寬製程技術。

在此次的研究中，側壁堆疊閘極法搭配適當的閘極蝕刻深度可以得到汲極飽和電流密度為 620 mA/mm，而電流在 1.5 V 的汲極偏壓下最大的互導係數可達 930 mS/mm。元件的電流增益截止頻率以及最大震盪頻率分別為 130 GHz 與 200 GHz。雜訊方面，160 μm 的元件在 16 GHz 的頻率下，雜訊值為 0.69 dB 以及 9.76 dB 的增益值。此外，

在功率特性方面， $160\ \mu\text{m}$ 的元件於 $2.4\ \text{GHz}$ 下，最大輸出功率為 $17.76\ \text{dBm}$ ($365\text{mW}/\text{mm}$)，功率增益為 57.7% ，其線性增益為 $27.83\ \text{dB}$ 。因此，已證實九十奈米側壁閘極應用於砷化鎵變異結構高電子遷移率電晶體具有相當好的高射頻特性。



High RF Performance GaAs Metamorphic HEMTs with 90 nm Sidewall Gate

Student: Yi Hsuan Peng

Advisor: Dr. Edward Yi Chang

**Institute of Materials Science and Engineering
National Chiao Tung University**

Abstract

For high frequency applications, the requirement of short gate length is necessary to improve the RF performance of the devices. The main purpose of this dissertation is to shrink the gate length with sidewall gate process. By sequentially depositing and selectivity etching two different dielectric layers (SiN_x and SiO_x), the nano-scale T-shaped gate was successfully fabricated. This technology can provide high reproducibility and uniformity due to the high etching selectivity between SiN_x and SiO_x . Finally, we developed a well-controlled gate technology for the fabrication of GaAs Metamorphic HEMTs with gate length below 100 nm.

The fabricated 90nm MHEMTs with optimum gate recess width has a saturation drain current of 620 mA/mm and a maximum transconductance of 930 mS/mm measured at $V_{ds}=1.5$ V. The device demonstrates a cutoff frequency f_T of 130 GHz and a maximum

frequency of oscillation f_{max} up to 200 GHz. The noise figure of the $160\ \mu\text{m}$ device is 0.69 dB and the associated gain is 9.76 dB at 16 GHz. The device also exhibits an output power of 17.67 dBm which is corresponding to a very high power density of 365 mW/mm. The maximum power-added efficiency is 57.7%, and the linear power gain is 27.83dB when measured at 2.4 GHz. In conclusion, a 90nm sidewall gate process is successfully developed and applied to the fabrication $\text{In}_{0.52}\text{Al}_{0.48}\text{As}/\text{In}_{0.52}\text{Ga}_{0.48}\text{As}$ metamorphic HEMTs with good RF performance, device reproducibility and uniformity.



致謝

今天能完成這本碩士論文,首先要感謝我的指導教授張翼老師,在實驗上提供我們如此豐富的資源,以及在研究上的熱心指導,沒有老師的強力支援,這本論文不可能如此順利完成。

另外,也感謝陳仕鴻、張晃崇、連亦中、褚立新、吳偉誠、徐金鈺、黃瑞乾、郭建億、張家源學長以及陳柏舟學弟,在實驗上及學問上的幫助與建議。研究所兩年的生活,大部分的時間都與實驗室的成員相處,我真的很開心能在實驗室遇到那麼多親切的朋友,就像一家人似的,可以一起分享喜怒哀樂一起玩樂一起打拼,我真的很珍惜這兩年來的研究生生涯,謝謝實驗室的你們對我如此照顧及包容,這兩年的點點滴滴都將是我最美好的回憶。

最後,要感謝我的家人及朋友,無怨無悔的全力支持我念研究所,無論是在精神上或是物質上的協助及鼓舞,都讓我能無後顧之憂全力衝刺,謝謝你們的支持與關懷,我才能順利的完成學業,真的非常謝謝你們!

Contents

Abstract (in Chinese)

Abstract (in English)

Acknowledgements

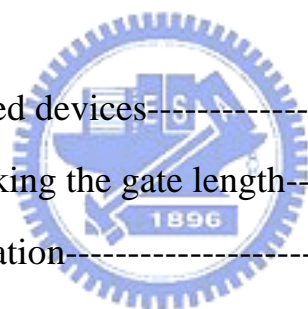
Contents

Table Captions

Figure Captions

Chapter 1 Introduction

1.1 Overview of high speed devices-----	01
1.2 Technologies of shrinking the gate length-----	04
1.3 Outline of this dissertation-----	06



Chapter 2 Dry etching characteristics of SiN_x and SiO_x

2.1 Etching system-----	15
2.2 Etching mechanisms-----	16
2.3 Etching selectivity-----	18
2.4 Etching experiment-----	19
2.5 Results and discussion-----	19

Chapter 3 Experiment and Basics of DC & RF characteristics

3.1 Device structure-----	31
3.2 Device fabrication-----	32
3.2.1 Mesa isolation-----	32
3.2.2 Ohmic contact formation-----	32
3.2.3 Sidewall T-shaped gate process -----	33
3.2.4 Gate recess-----	34
3.2.5 Device passivation and contact via formation-----	35
3.2.6 Airbridge formation-----	35
3.3 DC Characteristics-----	36
3.3.1 <i>I-V</i> characteristics-----	36
3.3.2 Transmission line model (TLM) -----	40
3.3.3 Breakdown characteristics-----	41
3.4 RF Characteristic & Measurements-----	42
3.4.1 Scattering parameters-----	42
3.4.2 Current gain cutoff frequency f_T -----	44
3.4.3 Maximum frequency of oscillation f_{max} -----	46
3.4.5 Noise figure-----	48
3.4.6 RF measurement calibration-----	50

Chapter 4 Results and Discussion

4.1 DC characteristics-----	69
4.1.1 <i>I-V</i> characteristics-----	69
4.1.2 Breakdown voltage-----	70
4.2 RF characteristics-----	70
4.2.1 Unit current gain cutoff frequency (f_T) & maximum frequency of	

oscillation (f_{max})	70
4.2.2 Noise characteristics	71
4.2.3 Power performance	72
4.3 Uniformity	73
4.4 Summary	74

Chapter 5 Conclusions

5.1 Conclusions	88
-----------------	----

References



Figure Captions

Chapter 1

Fig. 1.1 Energy band gap v. s. lattice constant for $\text{In}_x\text{Al}_{1-x}\text{As}/\text{In}_y\text{Ga}_{1-y}\text{As}$ system

Fig. 1.2 SEM photographs of the EB resist pattern for nanocomposite and conventional ZEP

Fig. 1.3 Cleaved cross section of a 30-nm T-gate.

Fig. 1.4 (a) Schematic cross-section view of the HEMT

(b) Cross-sectional TEM image of the 25-nm-long T-shaped gate

(c) Magnification of the TEM image around the bottom of the 25-nm-long T-shaped gate.

Fig. 1.5 T-gate process flows of the PSM technique

Fig. 1.6 Process flow of the thermally reflowed T-gate

Fig. 1.7 Sidewall gate diagram

Chapter 2

Fig. 2.1 Schematic diagram of the STS ICP

Fig. 2.2 Mechanism for plasma reaction

Fig. 2.3 Dry etching in F-based gases and plasmas

Fig. 2.4 Etching rates of SiN_x and SiO_x , and selectivity as a function of Ar flow

Fig. 2.5 Etching rates of SiN_x and SiO_x , and selectivity as a function of chamber pressure

Fig. 2.6 Etching rates of SiN_x and SiO_x , and selectivity as a function of RF power

Fig. 2.7 Etching rates of SiN_x and SiO_x , and selectivity as a function of ICP power

Fig. 2.8 Etching rates of SiN_x and SiO_x

Fig. 2.9 Surface roughness without plasma treatment

Fig. 2.10 Surface roughness with plasma treatment

Fig. 2.10 Breakdown voltage with and without plasma treatments

Chapter 3

Fig. 3.1 Cross-section structure of the MHEMT

Fig. 3.2 Ohmic contact resistance

Fig. 3.3 The dose dependence of the gate foot size of a single PMMA resist layer after development

Fig. 3.4 The dose dependence of the gate head size of a bi-layer (Copolymer/PMMA) resist layer after development

Fig. 3.5 Process flow of sidewall gate fabrication

Fig. 3.6 SEM photos of the sidewall gate process

Fig. 3.7 SEM photos of the sidewall T-shaped gate before and after gate metal deposition

Fig. 3.8 Process flow of airbridge

Fig. 3.9 SEM micrograph of the finished air-bridge profile

Fig. 3.10 Band diagrams at three different locations along the channel of a HEMT

Fig. 3.11 Actual characteristics and those predicted by Eq. (3-3)

Fig. 3.12 The TLM pattern

Fig. 3.13 The illustration of utilizing TLM to measure ohmic contact resistance

Fig. 3.14 The equivalent two-port network schematic at low frequency

Fig. 3.15 The equivalent two-port network schematic at high frequency

Fig. 3.16 Small signal representation of a common source FET

Fig. 3.17 CGS probe tips for the microwave measurement

Fig. 3.18 Different ISS substrates for the calibration

Fig. 3.19 Short, through and loads for the calibration

Fig. 3.20 Flow chart for the RF measurement calibration

Chapter 4



Fig. 4.1 SEM photos of sample A and sample B

Fig. 4.2 I - V characteristics of sample A and sample B

Fig. 4.3 Transconductance vs. applied voltage for sample A and sample B

Fig. 4.4 Breakdown voltage of sample A and sample B

Fig. 4.5 Cutoff frequency (f_T) vs. I_{ds} and V_{ds} of sample A and sample B

Fig. 4.6 Current gain, maximum available/stable power gain, and unilateral power gain of sample A and sample B

Fig. 4.7 F_{min} vs. I_{ds} at 16 GHz of sample A and sample B

Fig. 4.8 Noise figure (NF_{min}) and associated gain (G_a) vs. frequency of sample A and sample B

Fig. 4.9 Output power contours with a fixed input power of -5dBm at 2.4GHz for sample A

Fig. 4.10 P_{out} , gain and PAE of the sample A and sample B at 2.4GHz

Fig. 4.11 P_{out} , gain and PAE of the sample A and sample B at 6GHz

Fig. 4.12 The histogram of V_{th} and g_m across the wafer for sample A



Table Captions

Chapter 1

Table 1.1 Comparison of lattice-matched InP HEMT and metamorphic GaAs HEMT

Chapter 4

Table 4.1 Summary of the DC performances

Table 4.2 Summary of the RF and noise performances

Table 4.3 Summary of the power performances

